THE JOURNAL OF PHYSICAL CHEMISTRY C

Article

pubs.acs.org/JPCC

Molecular Dynamics Investigation of the Effects of Tip−Substrate Interactions during Nanoindentation

F. Tavazza,*[,†] T. P. Senftle,[‡] C. Zou,[§] C. A. Becker,[†] and A. C. T van Duin[§]

[†]Materials Science and Engineering Division, National Institute of Standards and Technology, 100 Bureau Drive, Gaithersburg, Maryland 20899, United States

[‡]Department of Chemical Engineering and [§]Department of Mechanical and Nuclear Engineering, Pennsylvania State University, University Park, Pennsylvania 16802, United States

Supporting Information

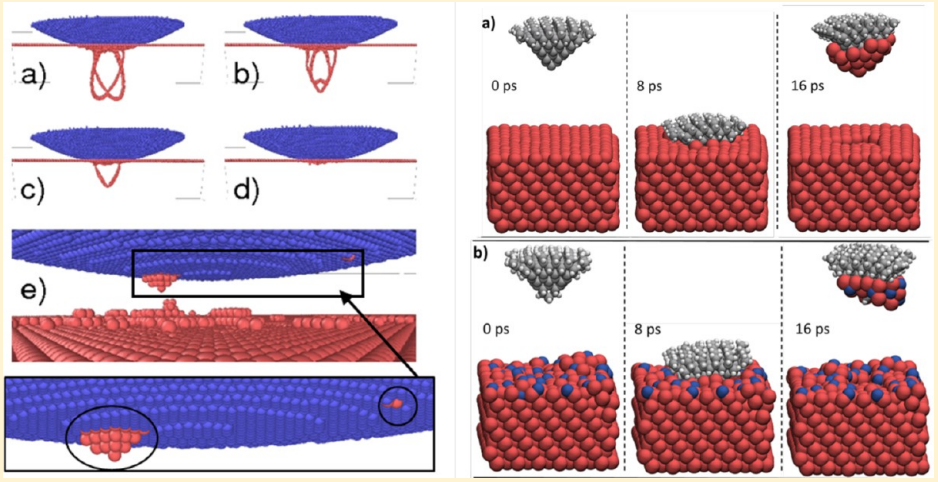

ABSTRACT: Nanoindentation in molecular dynamics (MD) simulations typically uses highly idealized indenter tip models. Such tips usually consist of either a single sphere or a collection of atoms, both of which are purely repulsive in their interactions with the substrate. It is also assumed that there is no environmental or substrate contamination, nor is there a surface oxide layer. In this work we examine the effects of these assumptions by comparing detailed MD simulations utilizing varying interaction potentials against both experimental atomic force microscopy observations and calculations using density functional theory. Specifically, we examine the effect of a tip−substrate interaction on the indenter under clean, hydrogenated, and oxidized conditions. We find that under clean or oxidized conditions (where we include oxygen on the nickel surface to mimic a passivating NiO layer) there is a substantial material transfer from the substrate to the tip. This material (Ni atoms) remains adsorbed on the tip upon retraction. However, the presence of hydrogen on the diamond tip drastically reduces, or even altogether eliminates, this material transfer, therefore having an effect much larger than that of a contaminating oxide layer.

1. INTRODUCTION

Nanoindentation is widely used to study the mechanical behavior of materials in the nanoscale regime.[1−4] By looking at load−displacement curves, researchers often infer how the material behaved under loading and unloading conditions. However, there are a number of ambiguities in the interpretation of the measurements. For example, experimental atomic force microscopy (AFM) images of indenter tips show significant blunting and irregularities after use.[5] As discussed in ref 5, the indenter blunting and irregular shape are directly visible in the AFM images and produce irregularities in the corresponding finite element method (FEM) simulations. Those FEM simulations used the AFM indenter profiles as a starting point and produced stress maps that, in the case of an intensively used indenter, showed several small areas of highly localized shear stress directly underneath the contact surface.

While the authors of ref 5 did not discuss the possibility of substrate adhesion to the tip, both experimental[6−8] and computational[9,10] work have shown that such adhesion is possible and, in fact, can be favorable under certain conditions. A recent "perspective" article[11] reviewed much of the previous understanding on atomistic-scale nanoindentation, including direct comparisons of experimental and computational work using field ion microscopy and molecular dynamics (MD). Specifically, adhesion of Au layers on W tips has been observed

Received: February 6, 2015
Revised: April 10, 2015
Published: May 8, 2015

DOI: 10.1021/acs.jpcc.5b01275
J. Phys. Chem. C 2015, 119, 13580−13589

in both experiment and computation.[12] However, the case of a W tip on the Au substrate was done under ultrahigh vacuum (UHV) conditions. While the importance of temperature and ambient conditions is mentioned,[6] the effects are not studied systematically.

Even though previous work has shown that dislocations nucleate with different mechanisms using a single large sphere versus an atomically resolved tip,[13] many recent nanoindentation simulations continue to use this methodology for performing nanoindents into a substrate. A simplistic repulsive interaction is also often used,[14] where the indenter (as a single large sphere or a crystal of "atoms") exerts a force on the substrate of the form

$$F(r) = -K(r - R)^2$$

where K is the specified force constant, r the distance from the atom to the center of the indenter, and R the indenter radius. MD simulations that follow these choices have the advantage of needing only a single-element force field (interatomic potential); however, they may miss important details in the evolution of the system.

The goal of this paper is to use MD to investigate how these assumptions affect observed results. We also want to determine if more realistic models, such as those described below, can aid in interpreting the AFM findings of ref 5. Specifically, we want to address the following questions:

- What is the extent of tip−substrate attraction, and how much does such an attraction affect simulation results?
- Does the tip deform or wear during nanoindentation? Is substrate adhesion a significant factor?
- What are the effects of environmental contaminants and surface oxides?

We will thus use a deformable indenter and examine (1) the effect of a purely repulsive tip−substrate interaction in the Ni−C system; (2) the same Ni−C interatomic potential with a density functional theory (DFT)-based Lennard-Jones term[15] that includes an attractive interaction; and (3) a ReaxFF[16] interatomic potential that includes reactive descriptions of nickel, carbon, hydrogen, and oxygen. Specifically, this last case allows us to test the effects of hydrogenation and an oxide layer at the nickel surface. We thus tested a clean nickel surface and clean diamond tip, a hydrogenated indenter tip on clean nickel, as well as the effect of an oxygen layer on the metal surface.

We will begin by outlining our methodology. This will be followed by a description of the fitting process for the EAM[17] nickel[18] and Tersoff carbon[19] potentials with a Lennard-Jones[15] tip−substrate (Ni−C) interaction. Then we will discuss the ReaxFF[20,21] potentials. After outlining the potentials used, we will discuss our simulation results and finish with a discussion of our findings.

2. SIMULATION CONDITIONS

In this work, we conduct several sets of MD simulations of nanoindentation.

In all cases, we indented into a (111)-oriented nickel substrate. This is the same geometry that was used in a comparison of nickel potentials previously published.[22] The indentation was performed with a diamond indenter tip. We used both a spherical indenter and one that was atomically sharp. The latter geometry was pyramidal (four faces), with each face cut along a (111) plane. In all simulations, the indenter was atomically stepped and deformable according to the defined atomic interactions between the carbon atoms.

A first set of simulations was run to perform the Ni−C fitting for the attractive part of the Lennard-Jones potential. In this case we used simulation procedures selected to mimic those of the DFT investigation of the early stages on nanoindentation that was used as a source of both fitting and validation data. As in the DFT calculations, here the nanoindentation was performed semistatically: we used the top of the indenter as a grip (9 Å thick), and we lowered it by 0.1 Å at each semistatic step. After the grip was lowered, and before the next semistatic step, we ran 50 000 MD steps (with a time step of 1 fs) to relax the system while keeping the indenter grip layer (9 Å thick) and the bottom of the Ni substrate (6 Å thick) fixed in their bulk positions.

The MD simulations were conducted in the *NVT* ensemble, where a Nose−Hoover thermostat[23] was employed. The overall system size we used was much larger than the one utilized in the DFT study, but we made sure to have an atomically sharp indenter (see Figure 1), exactly as used in the referenced DFT work. In the current study, the Ni substrate was 80 Å wide in the x direction, 79 Å in the y direction, and 50 Å thick. Periodic boundary conditions were used along the x and y directions. The indenter was 57 Å thick from the lowest C atom to the top of the grip. The entire configuration is shown in Figure 1. The initial distance between the indenter and the Ni surface was 1.825 Å. We decided to work at 300 K, instead of 0 K as in the DFT case, to have faster equilibration of the system at each step. A detailed investigation of the time convergence of the quantities of interest proved that 50 000 MD steps provided good convergence for all of them.

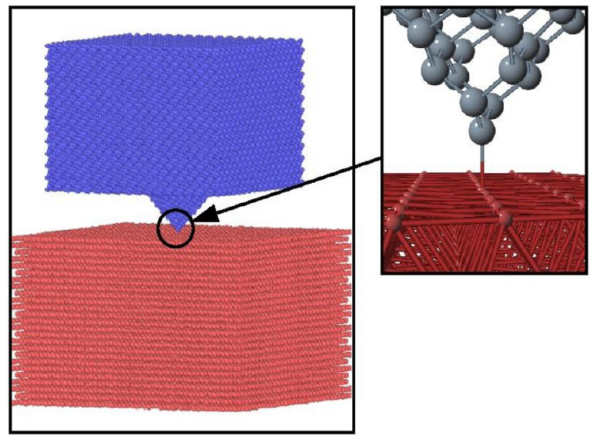

Figure 1. Simulation configuration used during the fitting of the Lennard-Jones potential for the Ni−C interaction. Carbon atoms are blue in the main figure and gray in the inset; Ni atoms are red in both.

Once a suitable potential was determined, we used it to examine nanoindentation phenomena. These simulations were performed differently from the ones used to fit the potential and are described individually below.

To investigate indenter wear and possible changes to the tip from interactions with the substrate, we used the hybrid potential described above to simulate indentation and retraction using an atomically carved, (100)-diamond spherical indenter, as created by the LAMMPS[24] code. The indenter had a radius of 298 Å, was 29 Å high, and included 358 266 atoms. The Ni substrate size was 500 × 500 × 200 Å^3, with periodic

DOI: 10.1021/acs.jpcc.5b01275
J. Phys. Chem. C 2015, 119, 13580−13589

boundary conditions along x and y, and a fixed bottom layer of 6 Å along z, for a total of 4 586 204 atoms. During this investigation, we compared results at two different temperatures: 1 and 300 K. We also investigated the effect of the indenter speed by running simulations at a "standard" speed of 0.1 Å/ps (10 m/s) and at a "slow" speed of 0.01 Å/ps (1 m/s). The "standard" speed is among the slowest speeds commonly used in MD nanoindentation simulations;[25−27] for instance, it was the slowest speed investigated in a paper focused on understanding the effects of the indenter speed on nanoindentation results.[28] We used a time step of 1 fs, and we indented to a depth of 11.5 Å before starting the indenter retraction.

The ReaxFF potential was employed to obtain a more detailed analysis of reactive interactions between the diamond indenter, the Ni surface, and ambient species such as oxygen and hydrogen. All ReaxFF simulations were conducted with an atomically sharp indenter tip consisting of four pyramidal (111)-sides carved from the bulk diamond structure, as was used in the analogous DFT study. The indenter structure consisted of 142 carbon atoms with 80 hydrogen atoms included to cap unsaturated carbon atoms at the indenter base, leaving the tip clean to assess Ni−C interactions at the indenter−surface interface. Two additional hydrogenated tip structures were also employed to assess the effect of hydrogen on the tip−surface interaction. One was a fully hydrogenated indenter, where hydrogen atoms were added to the system until every carbon atom was fully saturated in a tetrahedral configuration (a total of 120 H atoms). The second was a partially hydrogenated indenter with hydrogen atoms bonded to the 7 bottommost carbon atoms at the indenter tip, leaving the carbon atoms in the middle region of the indenter unsaturated (a total of 87 H atoms). All simulations employed a 25.83×29.82 Å^2 Ni(111) surface that was 8 Ni layers thick and was periodic in the x and y directions (resulting in a total of 1152 Ni atoms). An oxygenated surface was also constructed, where surface oxygen atoms were added to the Ni surface via a previously described[29] grand canonical Monte Carlo−molecular dynamics (GC-MC/MD) simulation scheme. During the GC-MC/MD simulation, oxygen atoms from a thermodynamic reservoir are inserted into and removed from the system using the Metropolis criterion[30] to accept or reject MC moves. A MD relaxation of forces is employed at each MC iteration prior to applying the Metropolis acceptance criterion, thus allowing the Ni surface to restructure while accommodating inserted oxygen atoms. The converged system structure thus consists of a surface oxide in equilibrium with an oxygen gas phase at the temperature and pressure of the reservoir, which was chosen as T = 300 K and P_{O_2} = 0.1 atm to reflect typical ambient conditions. This results in a surface oxide containing 58 oxygen atoms per 144 surface Ni atoms. The indenter and surface structures employed during ReaxFF MD simulations are shown in Figure 2.

All ReaxFF MD simulations were conducted in the *NVT* ensemble, where a Berendsen thermostat[31] with a 500 fs damping constant was employed to maintain a system temperature of 300 K. An extended Ni surface surrounding the indentation site precludes lateral expansion, as the entire Ni slab would have to expand uniformly. Hence, simulations in the *NVT* ensemble are appropriate as they do not allow for the dissipation of surface stress by an unphysical uniform expansion of the entire Ni surface. Each simulation consisted of 70 000 MD iterations with a time step of 0.25 fs, yielding a total simulation time of 17.5 ps. In all simulations, the indenter tip was initially placed 17.6 Å above the Ni surface and was lowered at a rate of 2.4 Å/ps for the initial 35 000 iterations and was retracted at the same rate for the final 35 000 iterations. This yields a penetration depth of 3.4 Å below the Ni surface, which corresponds to three Ni atomic layers. The position of the indenter was controlled via bond restraints between fixed dummy atoms (four placed above and two below the surface) and four carbon atoms at the indenter base and two at the tip. A total of six MD simulations were conducted, consisting of the three indenter models interacting with each of the two surface models, allowing for a comparative analysis of the various effects hydrogen and oxygen contaminates have on Ni−C interactions at the indenter−surface interface.

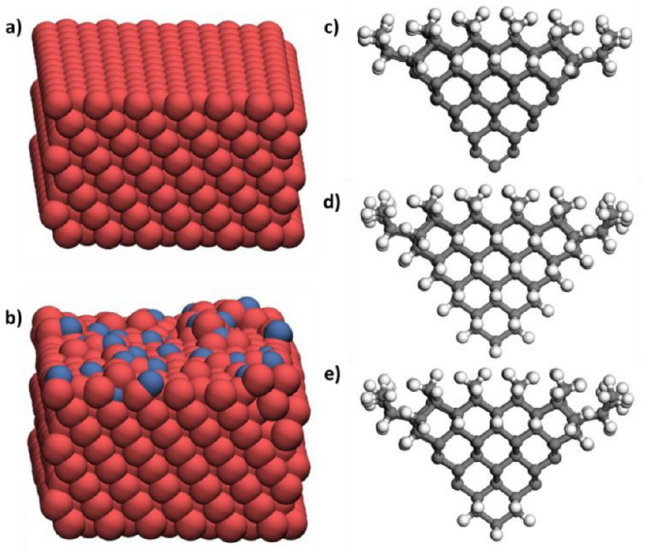

Figure 2. Surface and indenter structures used during ReaxFF MD simulations. (a) Clean and (b) oxidized Ni surface structures; Ni are light-red and O atoms are blue. (c) Clean, (d) fully hydrogenated, and (e) partially hydrogenated diamond indenter structures; C atoms are gray, and H atoms are white.

All hybrid potential simulations were run using LAMMPS,[25] while the ReaxFF simulations were conducted using a standalone FORTRAN code developed in the van Duin group.

3. INTERATOMIC POTENTIALS

3.1. Ni−C Lennard-Jones Attractive Interaction. Among the objectives of this work was the investigation of whether MD simulations can shed some light on the AFM experimental findings[5] of indenter tip damage after repeated use. To achieve this goal, we needed to use a deformable indenter in our simulations. We also needed an interaction as complete as possible between the indenter and the substrate. This meant including attractive and repulsive terms in the classical potential describing the indenter, the substrate, and their interactions. As we specifically investigated the case of a (111)Ni slab indented by a (100) diamond tip, this translated into using a potential that could offer good Ni−Ni, C−C, and Ni−C descriptions.

On the basis of previous experiences modeling nickel slabs and surfaces,[32] we decided to use a hybrid potential consisting of the 2004 Mishin nickel[18] potential to model the Ni−Ni interactions, the Tersoff carbon[19] potential to model C−C

DOI: 10.1021/acs.jpcc.5b01275
J. Phys. Chem. C 2015, 119, 13580−13589

bonds, and, finally, a Lennard-Jones[15] term to describe the mixed Ni−C interactions. Using a purely repulsive Lennard-Jones term to model an A−B interaction is fairly straightforward because the only parameter needed is the A−B equilibrium distance. However, including an attractive term (i.e., fitting the energy minimum) requires more information. To obtain such data, we ran specific DFT simulations of early stages of nanoindentation. These were semistatic simulations; therefore, for each fixed indenter−sample distance, the system (indenter and Ni slab) was completely relaxed. We fit the attractive contribution in the Lennard-Jones potential so that as the indenter tip approached the Ni surface, the displacement of Ni atoms toward the indenter matched what was observed in DFT simulations (Figure 3). Our DFT calculations gave a Ni−C equilibrium distance of 1.61 Å for the Ni−C dimer, but we decided instead to use as fitting distance the average Ni−C equilibrium distance obtained from the DFT simulations of very early stages of nanoindentation, 1.7 Å, as shown in Figure 3. This better reflects the multiple bond configurations of both C and Ni in our applications.

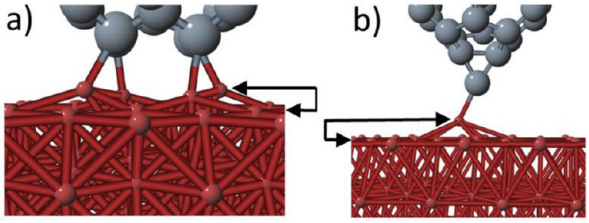

Figure 3. Examples of DFT fitting data. The arrows indicate the attraction effect that was used to fit the attractive part of the Ni−C Lennard-Jones potential. The smaller (red) spheres represent Ni atoms, while the larger (gray) are the C atoms.

Table 1 displays our parameters for the Ni−C Lennard-Jones potential, as implemented in LAMMPS. It is important to clarify that this hybrid potential was fit only to perform these nanoindentation simulations. It has not been tested in different situations, and it should not be used to simulate other physical properties without proper investigation.

Table 1. Calculated Equilibrium Ni−C Distance and Fitted Parameters for the Ni−C Lennard-Jones Interatomic Potential

DFT Ni−C distance (Å)	ε (eV)	σ (Å)	cutoff (Å)	shift parameter in LAMMPS
1.7	0.2	1.514	2.5	yes

3.2. ReaxFF Potential. The classical ReaxFF potential[16] is capable of describing complex covalent interactions between atoms during the process of forming and breaking bonds. It was originally developed to treat hydrocarbon systems, and its formalism has since been extended to handle metal and metal-oxide systems. This makes ReaxFF an ideal potential for assessing reactive Ni−C interactions in which Ni−C bonds are formed and broken at the indenter−surface interface in the presence of oxygen or hydrogen.

The force field used for this study is based on a previously developed Ni/C/O/H ReaxFF description[20] with substantial improvement and extension. The force field as reported in ref 20 was developed to describe the metallic nickel bulk and surface properties and hydrocarbon binding on nickel surfaces. The carbon parameters in that force field were improved to better describe the mechanical properties of graphene and diamond structures.[33] This improvement is critical for correctly predicting the performance of carbon-based indenters. The force field is further extended to describe the interstitial diffusion of oxygen impurities, along with their interaction with vacancies in bulk nickel and nickel oxide.[34] Lastly, a DFT data set consisting of carbon monoxide/dioxide binding on the Ni(111) surface (as described in ref 21) was included in the training process of the force field extension.

Force field training results for this last extension are provided in the Supporting Information. Although, this extension is not directly relevant to the systems in this study, it facilitates the continuous development and contributes to the transferability of the force field. This parameter set is available in ReaxFF input format in the Supporting Information.

Although computationally more expensive than the hybrid potential described above, ReaxFF can capture unique covalent contributions to the atomic interactions beyond the simple repulsive−attractive interactions captured by the simple hybrid potential. This will allow for a more detailed investigation of the nanoindentation process in the presence of contamination in the form of surface oxide formation or tip hydrogenation compared to the ideal clean indenter−surface interaction.

4. RESULTS

4.1. Purely Repulsive versus Attractive-and-Repulsive Tip−Substrate Interaction (Hybrid Potential). To better understand the effect of including an attractive term in the description of the indenter−substrate interaction, we simulated early stages of nanoindentation both with and without such a contribution. The Ni−Ni and C−C interaction descriptions are identical in both cases.

Figures 4a) and 4b) display the behavior we typically found when the Ni−C (substrate−indenter) interaction is purely repulsive. As the indenter tip begins penetrating into the Ni surface, the lowest-energy configuration makes room for penetrating C atoms by "ejecting" Ni atoms from the substrate.

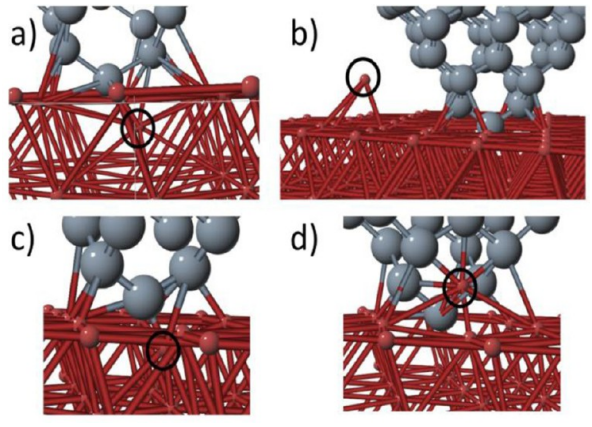

Figure 4. System evolution as the tip is lowered onto the substrate. If the Ni−C interaction is only repulsive, configurations a and b are obtained. Panel a shows the system just before a Ni atom (circled in the figure) is ejected, while panel b shows the same system just after such an ejection. The ejected Ni atom is pushed away from the indenter tip. If an attractive contribution is added into the mixed interaction, a Ni atom is similarly ejected (c), but its relaxed position is attached to the indenter (d).

DOI: 10.1021/acs.jpcc.5b01275
J. Phys. Chem. C 2015, 119, 13580−13589

Figure 4a displays a configuration just before such ejection took place. Figure 4b corresponds to the next semistatic step: a Ni atom has left the interior of the sample and moved to the surface, away from the indenter. If an attractive contribution is included in the mixed interaction, the deformation starts identically: a Ni atom is ejected to make room for the descending indenter tip (Figure 4c). However, the final location of the ejected atom is substantially different (Figure 4d): now the Ni remains in close proximity of the indenter. In these studies, the main relaxation mechanism during the very early stages of nanoindentation is the same for an only repulsive or repulsive-and-attractive description of the indenter−substrate interaction, but the details of the system evolution are clearly different.

We also compared our classical results to DFT simulations. In Figure 5 we show two snapshots of the DFT simulations of

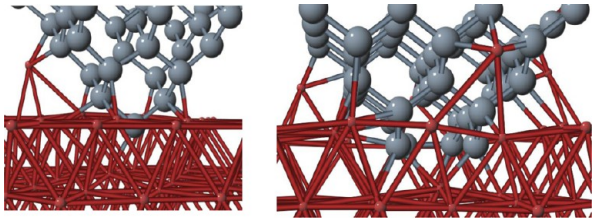

Figure 5. DFT simulations of early stages of nanoindentation. In both snapshots (corresponding to indentation made with two different indenter tips) Ni atoms that moved from the inside of the substrate to the surface, and ended up attached to the indenter, are clearly noticeable.

early stages of nanoindentation, one for an atomically sharp indenter and another where four atoms formed the indenter tip. These, and any other DFT configuration at this stage of indentation, were not included in the fitting process. In both configurations, Ni atoms have moved from the inside of the substrate to the surface and ended up attached to the indenter, as seen in our MD simulations. Therefore, adding the Ni−C attraction to the classical description of the Ni−C interactions produces a system evolution in excellent qualitative agreement with DFT results.

4.2. Indenter Deformation (Hybrid Potential Results). Because the primary goal of this work was to use MD tools to understand the experimentally reported findings of indenter wear and possible contamination, we started by using the hybrid potential described above and simulated one cycle of indentation and retraction.

Figure 6 displays our findings for a temperature of 1 K and indenter speed of 0.1 Å/ps (10 m/s). We indented to a depth of 11.5 Å, then retracted the indenter. As Figure 6 shows, after complete retraction we find Ni atoms forming small pile-ups on the surface. Figure 6b more clearly displays the nature of such pile-ups: numerous single Ni atoms are scattered on the surface where the indenter made contact, with a few larger structures, at most three layers thick. Figure 6b also shows that one Ni atom has attached to the indenter and is completely disconnected from the Ni substrate. This finding is not enough to clearly indicate whether or not there is Ni adhesion on the diamond indenter as a result of the indentation cycle.

To better understand what happens at this very low temperature, we ran similar simulations using an indenter speed 10 times slower. It is well-known that indenter speeds used in MD simulations are much faster than those in

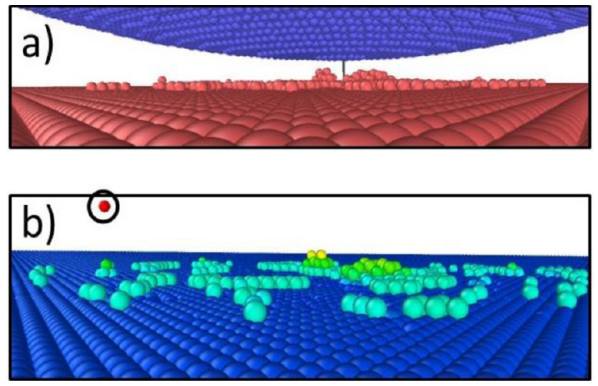

Figure 6. (a) Ni substrate (red) and indenter tip (blue) after the indenter has been completely pulled out of the nickel. Simulation conditions: T = 1 K; indenter speed of 0.1 Å/ps ("fast"). In panel b, only Ni atoms are shown. They are color coded with respect to their z coordinate, going from dark blue, which corresponds to the Ni surface (z = 0 Å), to red, which indicates the only Ni atom that has attached to the indenter (z = 16 Å).

experiments, so it is important to investigate the effect such a computational parameter has on the simulation results. Figure 7

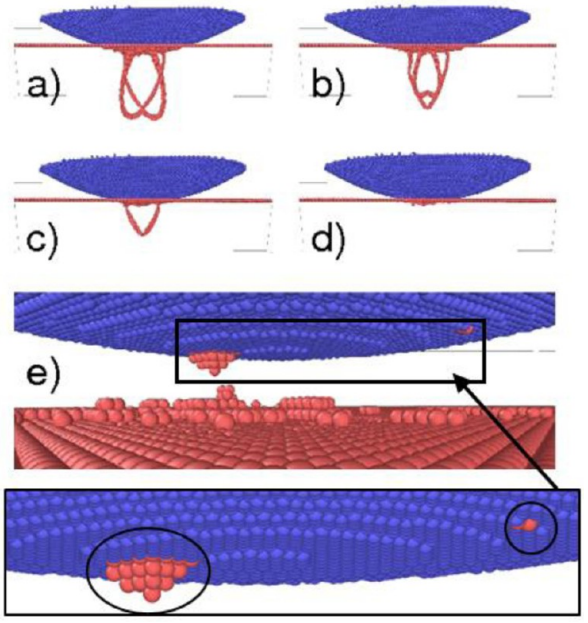

Figure 7. System evolution as a "slow" indenter (speed = 0.01 Å/ps) is retracted after an indentation 11.5 Å deep at T = 1 K: (a) maximum indentation depth, (b) depth = 10.5 Å, (c) depth = 5.5 Å, and (d) depth = 3.5 Å. In panels a−d, only Ni atoms with centrosymmetry parameter larger than 3 are shown (red). In panel e, the indenter (blue) is completely detached from the Ni substrate (red) and Ni pile-ups can be seen on both the Ni surface and the indenter tip.

shows the evolution of the system as the indenter is retracted after having indented to a depth of 11.5 Å (as in the previous case). Only Ni atoms with a centrosymmetry parameter larger than 3 are shown (red). As the indenter is retracted, the system recovers and displacements due to dislocation nucleation "heal" (Figure 7 a-d). However, as the indenter is completely removed from the Ni sample, Ni pile-ups can be seen on both the Ni surface and the indenter tip. The size of the pile-up(s) on the tip leaves no doubt that significant tip adhesion (contami-

DOI: 10.1021/acs.jpcc.5b01275
J. Phys. Chem. C 2015, 119, 13580−13589

nation) may occur, even at such low temperatures, as a result of repeated indenter cycles, at least for this set of interactions.

We repeated the same investigation at room temperature (T = 300 K). Again, we used a 0.01 Å/ps (1 m/s) indenter speed, which is slower than what is often used in similar nanoindentation simulations.[26−29] In this case, the retraction of the indenter did not lead to a complete recovery of the original structure (Figure 8a,b), though a significant decrease in the

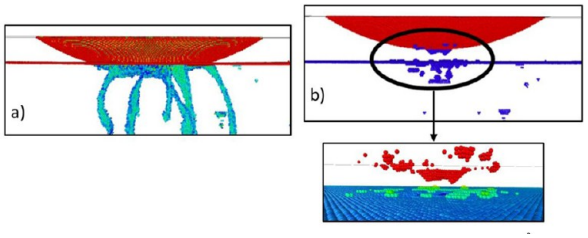

Figure 8. Initial (a) and final (b) configurations during a "slow" (speed = 0.01 Å/ps) indenter retraction at T = 300 K. Only Ni atoms (blue) with centrosymmetry larger than 3 are shown. The inset in panel b shows Ni atoms on and above the Ni surface. They are color coded with respect to their z coordinate, going from blue, corresponding to the Ni surface (z = 0 Å), to red, indicating Ni atoms that have attached to the indenter.

structural defects was still observed. As the indenter is completely retracted, a large amount of Ni is observed on the indenter tip (Figure 8b and inset). This amount is much larger than what was observed in the T = 1 K case for the same indentation speed.

Figure 9 allows direct comparison of the substrate adhesion to the indenter and to the Ni surface in the three cases that we have investigated with the hybrid potential. Only Ni atoms are shown in this figure, and they are color coded with respect to their z coordinate: the darkest blue indicates atoms 4 Å below the Ni surface; light blue indicates the Ni surface itself (z = 0 Å); light green and yellow indicate Ni atoms forming low pile-ups over the surface; and, finally, red indicates Ni atoms that have attached to the indenter. For the T = 1 K cases (Figure 9 a,b), a slower indenter speed (Figure 9b) causes the formation of larger pile-up "islands" and, correspondingly, larger areas where Ni atoms have been extracted from the sample, compared to the "standard" indenter speed case (Figure 9a). More Ni atoms have also attached to the indenter (indicated in red), forming one medium sized contamination "spot" and a small one. As the temperature is raised (Figure 9c,d), significant pileups are observed in the areas surrounding the impact point (in good agreement with what is observed in larger-scale indentation experiments), and directly under the indenter, we find comparatively large areas where Ni atoms have been extracted from the sample and attached to the indenter tip. All of these results are consistent with the larger atomic mobility that comes with having a higher temperature. Figure 9d depicts a clearer image of the Ni surface immediately under the indenter tip and shows that Ni atoms attached to the indenter tend to aggregate and form very ordered structures.

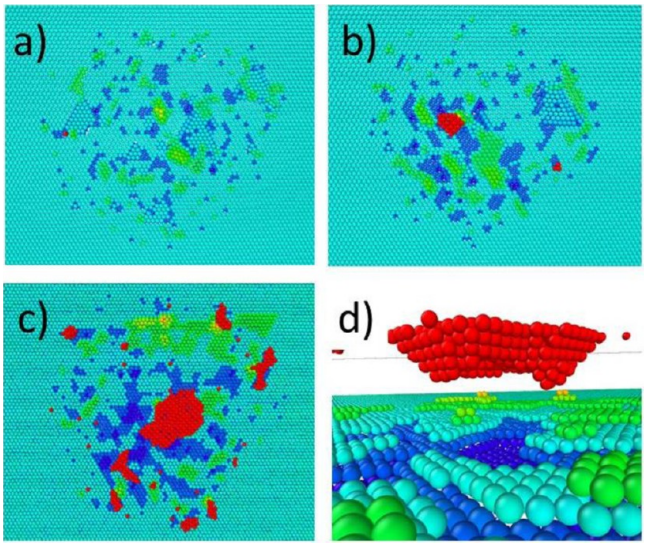

Figure 9. Top view of our system after the indenter has been completely retracted. Only Ni atoms are shown, color coded with respect to their z coordinate, going from dark blue, corresponding to 4 Å below the Ni surface, light blue for the Ni surface (z = 0 Å), to red, indicating Ni atoms that have attached to the indenter. Configuration a corresponds to the "standard" indenter speed, T = 1 K case; configuration b corresponds to the "slow" indenter speed, T = 1 K case; and configurations c and d correspond to the "slow" indenter speed, T = 300 K case.

To summarize what we have learned from the analysis of these three cases, indentation cycles likely induce indenter damage through indenter tip contamination. This contamination seems to occur even at very low temperatures if a slow enough indenter speed is used (which still is orders of magnitude faster than experimental speeds). However, none of our simulations have shown significant structural reorganization in the diamond indenter itself.

4.3. ReaxFF Potential Results for the Clean, Hydrogenated, and Oxidized System. The ReaxFF potential was employed to obtain a more detailed analysis of indenter−surface interactions in the presence of oxygen or hydrogen on the indenter or surface. Indentation simulations, summarized in Figures 10−12, consisted of a single indentation-retraction cycle using various combinations of tip or surface species. Figures 10 and 11 show trajectory snapshots of the initial (0 ps), middle (8 ps), and final (16 ps) system geometries during indentation simulations over the clean and oxidized Ni(111) surfaces, respectively. A video of each simulation is also provided in the Supporting Information. Figure 12 summarizes the total system energy during each simulation, where the energies are reported relative to the average energy of the system over the initial 3 ps before the indenter interacts with the surface.

A strong Ni−C interaction dominates the first indentation−retraction cycle in the absence of any contaminant, as seen in Figure 10a. This is further evident in Figure 12, where the total system energy decreases as the clean indenter approaches the Ni surface, indicating a net attractive force between the indenter and the surface. This is caused by Ni−C bonds formed between unsaturated C atoms and the Ni surface. The system energy briefly rises as surface Ni atoms are displaced into surrounding Ni atoms and then decreases again as the indenter retraction phase begins. As seen in the previous section with the hybrid potential, Ni atoms remain bonded to the diamond indenter after it is retracted away from the surface. The indenter−surface interaction is very different when hydrogen is present on the indenter, as shown in Figure 10b,c. For both the fully and partially hydrogenated indenters, there is no attraction to the surface at the onset of the indenter−surface interaction,

DOI: 10.1021/acs.jpcc.5b01275
J. Phys. Chem. C 2015, 119, 13580−13589

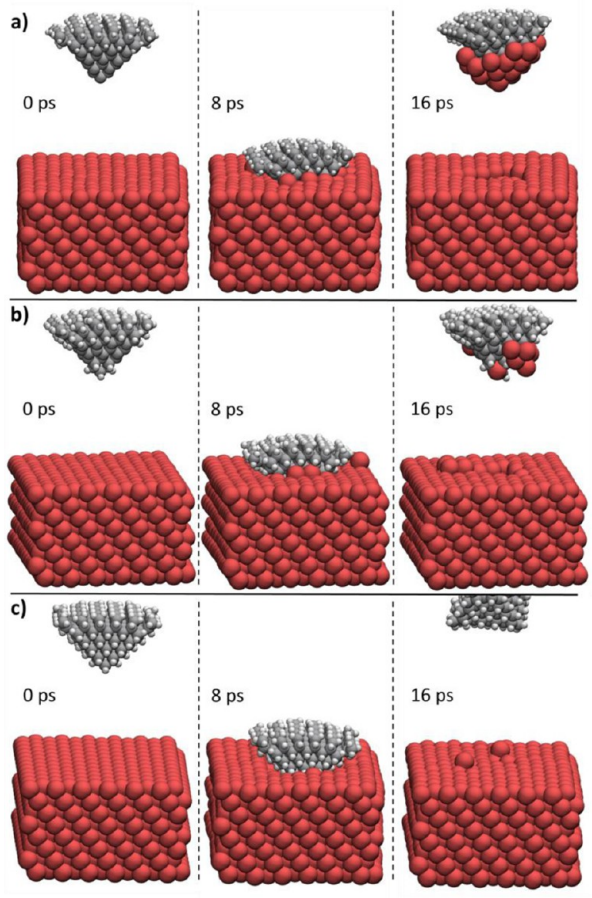

Figure 10. MD trajectory snapshots at 0 ps (left-hand panels), 8 ps (center panels), and 16 ps (right-hand panels) of ReaxFF indentation simulations on a clean Ni(111) surface using a (a) clean indenter, (b) partially hydrogenated indenter, and (c) fully hydrogenated indenter. Ni atoms are red, carbon atoms gray, and hydrogen atoms white.

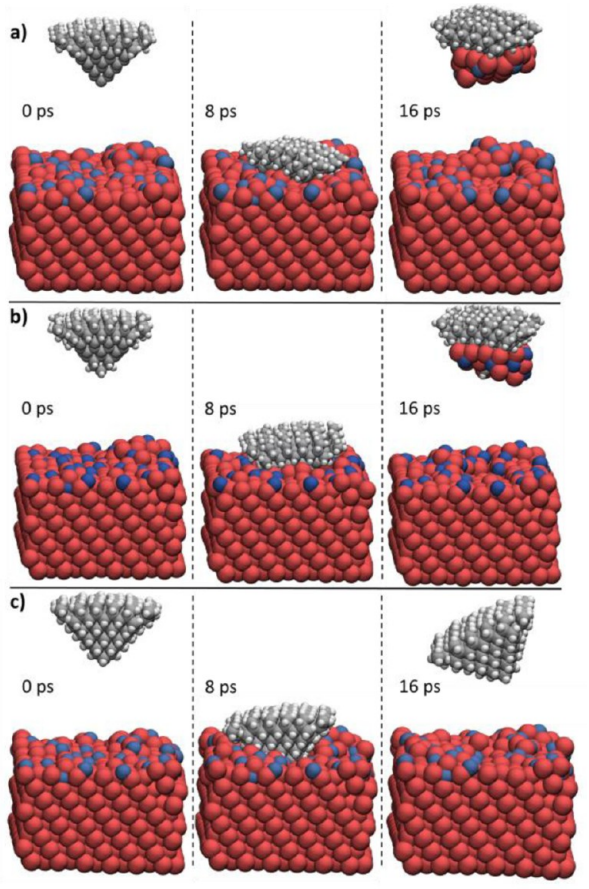

Figure 11. MD trajectory snapshots at 0 ps (left-hand panels), 8 ps (center panels), and 16 ps (right-hand panels) of ReaxFF indentation simulations on an oxidized Ni(111) surface using a (a) clean indenter, (b) partially hydrogenated indenter, and (c) fully hydrogenated indenter. Ni atoms are red, carbon atoms gray, hydrogen atoms white, and oxygen atoms blue.

evident in the increase in system energy seen in Figure 12. In the fully hydrogenated case, no Ni−C interactions are present, as every carbon atom is already fully hydrogenated, and displaced Ni atoms migrate away from the indenter leaving vacancies and Ni adatoms on the surface after retraction. As expected, the partially hydrogenated indenter behaves in a manner similar to the clean indenter when unsaturated carbon atoms reach the Ni surface, where the strong Ni−C interaction is evident in the decrease in system energy at 8 ps compared to the fully hydrogenated indenter. In this case, displaced Ni atoms are both left on the surface and attached to the indenter after retraction.

Similar indenter−surface interaction behaviors are observed in the presence of an oxide contamination layer: again we find Ni atoms that remain bonded to the diamond indenter after retraction for clean and partially hydrogenated tips, but not for the completely hydrogenated case. This overall similarity is evident in both the trajectory snapshots and system energy profiles. However, there are small differences that result from the disordered nature of the Ni-oxide surface, which could affect the interpretation of experimental data. The clean indenter displays a stronger net attraction to the oxidized surface, demonstrated in Figure 12b by the lower system energy at ≈9 ps compared to the analogous simulation over the clean surface. There is also a lower net repulsion between the hydrogenated indenter and the oxidized surface. The stronger attractive interaction occurs over the oxidized surface compared to the clean surface because it is energetically unfavorable to disrupt the close-packed Ni atoms in the clean surface. This is shown in Figure 12a, as the net change in system energy is always positive after the retraction phase. This increase in energy is mitigated over the oxidized surface, which is demonstrated in Figure 12b when the net change in system energy returns to zero after the surface interacts with the fully hydrogenated indenter.

These results demonstrated the utility of the ReaxFF potential for describing unique repulsive−attractive interactions that can affect results obtained from nanoindentation experiments. They demonstrate that strong Ni−C interactions result from reactive unsaturated carbon atoms present in atomically sharp indenters, which can lead to indenter contamination and sample destruction in the form of Ni vacancies. Furthermore, the presence of hydrogen can shield the indenter tip by saturating the most reactive carbon sites that would otherwise interact too strongly with the surface. Indeed, it is likely that the Ni vacancies created by the fully hydrogenated indenter over the clean surface could be avoided at slower indentation speeds, suggesting that hydrogenation could be a useful strategy for synthesizing nonreactive atomically sharp indenter tips.

DOI: 10.1021/acs.jpcc.5b01275
J. Phys. Chem. C 2015, 119, 13580−13589

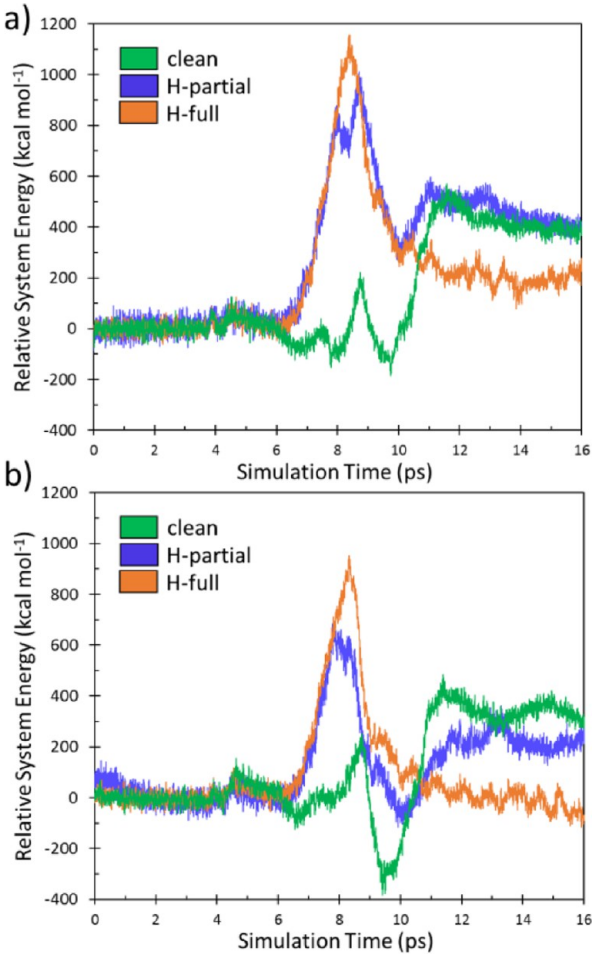

Figure 12. Relative system energies during ReaxFF indentation simulations on the (a) clean and (b) oxidized Ni(111) surface. Green data corresponds to simulations conducted with the clean indenter, blue data to simulations conducted with the partially hydrogenated indenter, and orange data to simulations conducted with the fully hydrogenated indenter.

5. DISCUSSION

Of the many parameters that affect the results of MD nanoindentation simulations, the most important is obviously the force field. Depending on the object of the investigation, a suitable force field must be chosen. Complex force fields, like ReaxFF, allow for a more realistic investigation of nanoindentation processes, as they allow the simulation of realistic features like oxide layers over the metallic surface and saturated carbon bonds. This ability is, however, balanced by their computational cost, which is much higher than that of simpler force fields, such as EAM, Tersoff, or Lennard-Jones. This higher computational cost may require the use of smaller computational cells and may, therefore, affect the results by not including long-range relaxations as well as is allowed by the use of faster potentials. Because of such unknowns, validation of the applicability of any force field prior to the investigation of a specific physical phenomena is always needed.

In this work we used various, progressively more complex potentials to investigate the nanoindentation process. Specifically, we focused on understanding how much the attraction between tip and substrate matters and whether including more realistic tip−substrate interactions (as for saturated tips and/or oxidized surfaces) alters the evolution of the system.

We determined that including an attractive interaction between the tip and the metallic substrate is crucial if a clean indenter is used and information about indenter wear and substrate surface deformation are desired. In the case of an ideal (unsaturated) indenter tip, we found excellent qualitative agreement between results obtained using the simpler and faster hybrid EAM−Tersoff−Lennard-Jones potential and those obtained using the more involved ReaxFF potential, as long as an attractive Ni−C interaction is included. In both cases, we found adhesion on the tip (Ni atoms that remained bonded to the diamond indenter after it is retracted from the surface) and nonidealities on the Ni surfaces: Ni-atoms pile-ups, pits, Ni adatoms on the surface, etc. Good qualitative agreement with DFT findings for very early stages of nanoindentation further validate our results. For the purpose of this investigation, we can therefore conclude that the direct Ni−C interaction is sufficiently well described by the simpler, faster hybrid potential, as no major differences are found using the ReaxFF potential. Also, as ReaxFF has not previously been applied to nanoindentation, the agreement between its results and those of the hybrid potential and DFT simulations validates its applicability to this field.

The use of the ReaxFF potential also allowed us to investigate more realistic conditions, such as the case of a hydrogen-saturated indenter tip. Here we obtained a system evolution very different from that found for a clean indenter tip, demonstrating that strong Ni−C interactions result from reactive unsaturated carbon atoms present in atomically sharp indenters. The presence of hydrogen can shield the indenter tip by saturating the most reactive carbon sites that would otherwise strongly interact with the surface.

The differences in adsorption behavior for the hydrogenated tip versus the non-hydrogenated tip highlight the importance of environmental and chemical interactions in these systems. For example, different tip−substrate adsorption behavior could be seen under UHV conditions, if not enough hydrogen is available to saturate the tip or if additional species preferentially react with the hydrogen and effectively remove it from the tip, or with different materials (as with the tungsten indenter on gold[12]).

We also examined the presence of an oxide layer over the metal surface. It has been experimentally determined that oxygen passivation of Ni creates a number of surface structures that depend on oxygen pressure, temperature, ambient conditions, and surface orientation.[35−37] For Ni(111) at 300 K, only a few layers appear to form.[37] The simulated coverage is consistent with those findings, though possibly more disordered. We determined that all key behaviors observed in the presence of an oxide layer are very similar to those observed for a clean metal surface: again we find Ni adhesion to the diamond indenter after retraction for clean and partially hydrogenated tips, but not for completely hydrogenated tips.

Taking advantage of the fact that the hybrid potential is computationally inexpensive, we used it to investigate the effect of the indenter speed on our results. We determined that slower speeds yielded more Ni adhesion on the tips. Because experimental speeds are many orders of magnitude slower than what is used in MD, we consider our findings an indication that, possibly, some adhesion would be seen even in the case of saturated tips if much slower indentation speeds were employed. However, this should be examined further.

DOI: 10.1021/acs.jpcc.5b01275
J. Phys. Chem. C 2015, 119, 13580−13589

6. CONCLUSIONS

We investigated the role of attractive interatomic interactions as well as of ambient species (oxygen and hydrogen) on both tip and substrate in simulations of nanoindentation. We found that inclusion of attractive interactions between the indenter and substrate reproduced tip-wetting effects seen in experiments, DFT, and previous MD simulations for different materials. The presence of ambient species, however, can substantially reduce the wetting, as we found for the case of hydrogen saturation. This work demonstrates the importance of capturing the appropriate chemical interactions, even in large systems such as those characteristic of nanoindentation. Much more work is needed to fully understand all of the complex effects in this system, but it is clear that a purely repulsive interatomic potential describing tip−substrate interaction can fundamentally change the nature of the system evolution in these simulations.

■ ASSOCIATED CONTENT

Supporting Information

Comparison of the adsorption energy of CO and CO_2 on nickel (111) surface predicted by ReaxFF and DFT; ReaxFF Ni/C/O/H parameter set employed in this study provided in ReaxFF input format. The Supporting Information is available free of charge on the ACS Publications website at DOI: 10.1021/acs.jpcc.5b01275.

■ AUTHOR INFORMATION

Notes

The authors declare no competing financial interest.

■ REFERENCES

(1) M. F. Doerner, M. F.; Nix, W. D. A method for interpreting the data from depth-sensing indentation instruments. *J. Mater. Res.* **1986**, *1*, 601−609.

(2) Fisher-Cripps, A. C. *Nanoindentation*; Springer-Verlag: New York, 2002.

(3) Oliver, W. C.; Pharr, G. M. An improved technique for determining hardness and elastic modulus using load and displacement sensing indentation experiments. *J. Mater. Res.* **1992**, *7*, 1564−1583.

(4) Oliver, W. C.; Pharr, G. M. Measurement of hardness and elastic modulus by instrumented indentation: Advances in understanding and refinements to methodology. *J. Mater. Res.* **2004**, *19*, 3−20.

(5) Ma, L.; Morris, D. J.; Jennerjohn, S. L.; Bahr, D. F.; Levine, L. E. The role of probe shape on the initiation of metal plasticity in nanoindentation. *Acta Mater.* **2012**, *60*, 4729−4739.

(6) Paul, W.; Miyahara, Y.; Grutter, P. H. Implementation of atomically defined field ion microscopy tips in scanning probe microscopy. *Nanotechnology* **2012**, *23*, 335702.

(7) Paul, W.; Oliver, D.; Miyahara, Y.; Grutter, P. H. Transient adhesion and conductance phenomena in initial nanoscale mechanical contacts between dissimilar metals. *Nanotechnology* **2013**, *24*, 475704.

(8) Paul, W.; Oliver, D.; Miyahara, Y.; Grutter, P. H. FIM tips in SPM: Apex orientation and temperature considerations on atom transfer and diffusion. *Appl. Surf. Sci.* **2014**, *305*, 124−132.

(9) Song, J.; Srolovitz, D. J. Adhesion effects in material transfer in mechanical contacts. *Acta Mater.* **2006**, *54*, 5305−5312.

(10) Song, J.; Srolovitz, D. J. Mechanism for material transfer in asperity contact. *J. Appl. Phys.* **2008**, *104*, 124312.

(11) Paul, W.; Oliver, D.; Grutter, P. H. Indentation-formed nanocontacts: An atomic-scale perspective. *Phys. Chem. Chem. Phys.* **2014**, *16*, 8201−8222.

(12) Oliver, D.; Paul, W.; El Ouali, M.; Hagedorn, T.; Miyahara, Y.; Qi, Y.; Grutter, P. H. One-to-one spatially matched experiment and atomistic simulations of nanometer-scale indentation. *Nanotechnology* **2014**, *25*, 025701.

(13) Wagner, R. J.; Ma, L.; Tavazza, F.; Levine, L. E. Dislocation nucleation during nanoindentation of aluminum. *J. Appl. Phys.* **2008**, *104*, 114311.

(14) LAMMPS: LAMMPS online manual, "fix indent" command. http://lammps.sandia.gov/doc/fix_indent.html.

(15) Lennard-Jones, J. E. On the Determination of Molecular Fields. *Proc. R. Soc. London, Ser. A* **1924**, *106*, 463−477.

(16) Van Duin, A. C. T.; Dasgupta, S.; Lorant, F.; Goddard, W. A., III. ReaxFF: A Reactive Force Field for Hydrocarbons. *J. Phys. Chem. A* **2001**, *105*, 9396−9409.

(17) Daw, M. S.; Baskes, M. Embedded-atom method: Derivation and application to impurities, surfaces, and other defects in metals. *Phys. Rev. B: Condens. Matter Mater. Phys.* **1984**, *29*, 6443−6453.

(18) Mishin, Y. Atomistic modeling of the γ and γ'-phases of the Ni−Al system. *Acta Mater.* **2004**, *52*, 1451−1467.

(19) Tersoff, J. Modeling solid-state chemistry: Interatomic potentials for multicomponent systems. *Phys. Rev. B: Condens. Matter Mater. Phys.* **1989**, *39*, 5566−5569.

(20) Mueller, J. E.; van Duin, A. C. T.; Goddard, W. A., III. Development and Validation of Reaxff Reactive Force Field for Hydrocarbon Chemistry Catalyzed by Nickel. *J. Phys. Chem. C* **2010**, *114*, 4939−4949.

(21) Wang, S. G.; Cao, D. B.; Li, Y. W.; Wang, J. G.; Jiao, H. J. Chemisorption of CO_2 on Nickel Surfaces. *J. Phys. Chem. B* **2005**, *109*, 18956−18963.

(22) Becker, C. A.; Tavazza, F.; Levine, L. E. Implications of the choice of interatomic potential on calculated planar faults and surface properties in nickel. *Philos. Mag.* **2011**, *91*, 3578−3597.

(23) Nose, S. A unified formulation of the constant temperature molecular-dynamics methods. *J. Chem. Phys.* **1984**, *81*, 511−519.

(24) Plimpton, S. Fast Parallel Algorithms for Short-Range Molecular Dynamics. *J. Comput. Phys.* **1995**, *117*, 1−19.

(25) Fang, T.-H.; Wu, J.-H. Molecular dynamics simulations on nanoindentation mechanisms of multilayered films. *Comput. Mater. Sci.* **2008**, *43*, 785−799.

(26) Verkhovtsev, V.; Yakubovich, A. V.; Sushko, G. B.; Hanauske, M.; Solov'yov, A. V. Molecular dynamics simulations of the nanoindentation process of titanium crystal. *Comput. Mater. Sci.* **2013**, *76*, 20−26.

(27) Zhu, P. Z.; Fang, F. Z. Molecular dynamics simulations of nanoindentation of monocrystalline germanium. *Appl. Phys. A: Mater. Sci. Process.* **2012**, *108*, 415−421.

(28) Imran, M.; Hussaina, F.; Rashida, M.; Ahmad, S. A. Dynamic characteristics of nanoindentation in Ni: A molecular dynamics simulation study. *Chin. Phys. B* **2012**, *21*, 116201.

(29) Senftle, T. P.; Meyer, R. J.; Janik, M. J.; van Duin, A. C. T. Development of a ReaxFF Potential for Pd/O and Application to Palladium Oxide Formation. *J. Chem. Phys.* **2013**, *139*, 044109.

(30) Metropolis, N.; Rosenbluth, A. W.; Rosenbluth, M. N.; Teller, A. H.; Teller, E. J. Equation of state calculations by fast computing machines. *Chem. Phys.* **1953**, *21*, 1087−1092.

(31) Berendsen, H. J. C.; Postma, J. P. M.; van Gunsteren, W. F.; DiNola, A.; Haak, J. R. Molecular dynamics with coupling to an external bath. *J. Chem. Phys.* **1984**, *81*, 3684−3690.

(32) Becker, C. A.; Tavazza, F.; Trautt, Z. T.; Buarque de Macedo, R. A. Considerations for choosing and using force fields and interatomic potentials in materials science and engineering. *Curr. Opin. Solid State Mater. Sci.* **2013**, *17*, 277−284.

(33) Srinivasan, S. G.; Ganesh, P.; van Duin, A. C. T. Thermal Decomposition of a Large Fullerene: A Molecular Dynamics Study Using the ReaxFF Reactive Force Field. *J. Phys. Chem. A* **2015**, *119*, 571−580.

(34) Zou, C.; Shin, Y. K.; Liu, Z. K.; Fang, H. Z.; van Duin, A. C. T. Molecular dynamics simulations of the vacancy effect on the nickel self-diffusion, oxygen diffusion and oxidation initiation in nickel using the ReaxFF reactive force field. *Acta Mater.* **2015**, *83*, 102−112.

DOI: 10.1021/acs.jpcc.5b01275
J. Phys. Chem. C 2015, 119, 13580−13589

(35) Erdman, N.; Warschkow, O.; Ellis, D. E.; Marks, L. D. Solution of the p(2 × 2) NiO(111) surface structure using direct methods. *Surf. Sci.* **2000**, *470*, 1−14.
(36) Ciston, J.; Subramanian, A.; Kienzle, D. M.; Marks, L. D. Why the case for clean surfaces does not hold water: Structure and morphology of hydroxylated nickel oxide (111). *Surf. Sci.* **2010**, *604*, 155−164.
(37) Okazawa, T.; Nishizawa, T.; Nishimura, T.; Kido, Y. Oxidation kinetics for Ni(111) and the structure of the oxide layers. *Phys. Rev. B: Condens. Matter Mater. Phys.* **2007**, *75*, 033413.

DOI: 10.1021/acs.jpcc.5b01275
J. Phys. Chem. C 2015, 119, 13580−13589